

Learning Distortion Invariant Representation for Image Restoration from A Causality Perspective

Xin Li^{1*}, Bingchen Li^{1*}, Xin Jin², Cuiling Lan^{3†}, Zhibo Chen^{1†}

¹University of Science and Technology of China ²Eastern Institute for Advanced Study

³Microsoft Research Asia

{lixin666, lbc31415926}@mail.ustc.edu.cn, jinxin@eias.ac.cn,
culan@microsoft.com, chenzhibo@ustc.edu.cn

Abstract

In recent years, we have witnessed the great advancement of Deep neural networks (DNNs) in image restoration. However, a critical limitation is that they cannot generalize well to real-world degradations with different degrees or types. In this paper, we are the first to propose a novel training strategy for image restoration from the causality perspective, to improve the generalization ability of DNNs for unknown degradations. Our method, termed **Distortion Invariant representation Learning (DIL)**, treats each distortion type and degree as one specific confounder, and learns the distortion-invariant representation by eliminating the harmful confounding effect of each degradation. We derive our **DIL** with the back-door criterion in causality by modeling the interventions of different distortions from the optimization perspective. Particularly, we introduce the counterfactual distortion augmentation to simulate the virtual distortion types and degrees as the confounders. Then, we instantiate the intervention of each distortion with a virtually model updating based on corresponding distorted images, and eliminate them from the meta-learning perspective. Extensive experiments demonstrate the effectiveness of our **DIL** on the generalization capability on unseen distortion types and degrees. Our code will be available at <https://github.com/lixinustc/causal-IR-DIL>.

1. Introduction

Image restoration (IR) tasks [8, 9, 34, 53], including image super-resolution [12, 26, 45, 48, 58, 59], deblurring [43, 78], denoising [3, 25, 42], compression artifacts removal [30, 55], etc, have achieved amazing/uplifting performances, powered by deep learning. A series of back-

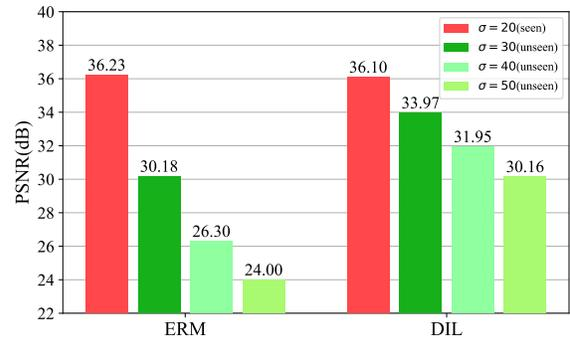


Figure 1. A comparison between ERM and our **DIL** with RRDB as backbone. The results are tested on the Set5 with gaussian noise.

bones are elaborately and carefully designed to boost the restoration performances for specific degradation. Convolution neural networks (CNNs) [21] and transformers [13, 36] are two commonly-used designed choices for the backbones of image restoration. However, these works inevitably suffer from severe performance drops when they encounter unseen degradations as shown in Fig. 1, where the restoration degree in training corresponds to the noise of standard deviation 20 and the degrees in testing are different. The commonly-used training paradigm in image restoration, *i.e.*, empirical risk minimization (ERM), does not work well for out-of-distribution degradations. Particularly, the restoration networks trained with ERM merely mine the correlation between distorted image I_d and its ideal reconstructed image I_o by minimizing the distance between I_o and the corresponding clean image I_c . However, a spurious correlation [46] is also captured which introduces the bad confounding effects of specific degradation d . It means the conditional probability $P(I_o|I_d)$ is also conditioned on the distortion types or degrees d (*i.e.*, $d \not\perp I_o|I_d$).

A robust/generalizable restoration network should be distortion-invariant (*i.e.*, $d \perp I_o|I_d$). For instance, given two distorted images with the same content I_c but different degradations d_1 and d_2 , the robust restoration network

*Equal contribution

†Corresponding Author

is expected to recover the same reconstructed image I_o from these two distorted images (i.e., $P(I_o|I_d, d = d_1) = P(I_o|I_d, d = d_2)$), respectively. Previous works for the robustness of the restoration network can be roughly divided into two categories, distortion adaptation-based schemes, and domain adaptation/translation-based schemes. Distortion adaptation-based schemes [62] aim to estimate the distortion types or representations, and then, handle the different distortions by adaptively modulating the restoration network. Domain adaptation/translation-based schemes [14, 37, 50] regard different distortions as different domains, and introduce the domain adaptation/translation strategies to the image restoration field. Notwithstanding, the above works ignore the exploration of the intrinsic reasons for the poor generalization capability of the restoration network. In this paper, we take the first step to the causality-inspired image restoration, where novel distortion invariant representation learning from the causality perspective is proposed, to improve the generalization capability of the restoration network.

As depicted in [18, 46], *correlation is not equivalent to causation*. Learning distortion invariant representation for image restoration requires obtaining the causal effects between the distorted and ideal reconstructed images instead of only their correlation. From the causality perspective, we build a causal graph for the image restoration process. As shown in Fig. 2, the distortions D including types D_t or degrees D_l are the confounders in IR, which introduces the harmful bias and causes the restoration process $I_d \rightarrow I_o$ condition on D , since a spurious relation path is established via $I_d \leftarrow D \rightarrow I_o$. The causal connection we want between distorted and ideal reconstructed image is $I_d \rightarrow I_o$, of which the causal conditional probability can be represented as $P(I_o|do(I_d))$. Here, a “do” operation [18, 46] is exploited to cut off the connection from the distortion D to I_d , thereby removing the bad confounding effects of D to the path $I_d \rightarrow I_o$, and learning the distortion-invariant feature representation (i.e., $D \perp\!\!\!\perp I_o|I_d$).

There are two typical adjustment criteria for causal effects estimation [18], the back-door criterion, and the front-door criterion, respectively. In particular, the back-door criterion aims to remove the bad confounding effects by traversing over known confounders, while the front-door criterion is to solve the challenge that confounders cannot be identified. To improve the generalization capability of the restoration network, we propose the **Distortion-Invariant representation Learning (DIL)** for image restoration by implementing the back-door criterion from the optimization perspective. There are two challenges for achieving this. The first challenge is how to construct the confounder sets (i.e., distortion sets). From the causality perspective [18, 46], it is better to keep other factors in the distorted image invariant except for distortion types. How-

ever, in the real world, collecting the distorted/clean image pairs, especially with different real distortions but the same content is impractical. Inspired by counterfactual [46] in causality and the distortion simulation [57, 74], we propose the counterfactual distortion augmentation, which selects amounts of high-quality images from the commonly-used dataset [2, 51], and simulate the different distortion degrees or types on these images as the confounders.

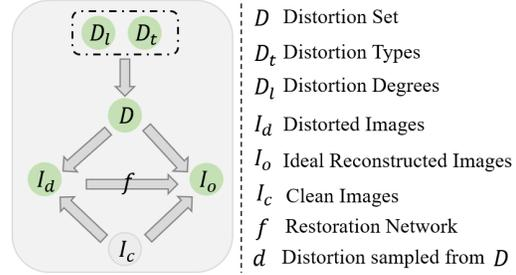


Figure 2. Causal structure graph for image restoration.

Another challenge of implementing DIL stems from finding a stable and proper instantiation scheme for back-door criterion. Previous works [38, 39, 56, 65, 67] have incorporated causal inference in high-level tasks by instantiating the back-door criterion [18] with attention intervention [65], feature interventions [68], etc, which are arduous to be exploited in the low-level task of image restoration. In this work, we theoretically derive our distortion-invariant representation learning **DIL** by instantiating the back-door criterion from the optimization perspective. Particularly, we model the intervention of simulated distortions for the restoration process by virtually updating the restoration network with the samples from the corresponding distortions. Then, we eliminate the confounding effects of distortions by introducing the optimization strategy from Meta Learning to our proposed DIL. In this way, we can instantiate the causal learning in image restoration and enable the **DIL** based on the back-door criterion.

The contributions of this paper are listed as follows:

- We revisit the image restoration task from a causality view and pinpoint that the reason for the poor generalization of the restoration network, is that the restoration network is not independent to the distortions in the training dataset.
- Based on the back-door criterion in causality, we propose a novel training paradigm, **Distortion Invariant representation Learning (DIL)** for image restoration, where the intervention is instantiated by a virtually model updating under the counterfactual distortion augmentation and is eliminated with the optimization based on meta-learning.
- Extensive experiments on different image restoration tasks have demonstrated the effectiveness of our **DIL** for improving the generalization ability on unseen distortion types and degrees.

2. Related Works

2.1. Image Restoration

Image Restoration (IR) [8, 24, 28, 34, 35, 53, 69] aims to recover high-quality images from the corresponding distorted images, which plays a prominent role in improving the human visual experience. With the advancement of deep learning, a series of works have achieved remarkable progress in lots of IR tasks, including image denoising [3, 42, 76], deblurring [43, 52, 78], super-resolution (SR) [10, 12, 29, 60, 63, 77], etc. Particularly, most of them are devoted to elaborately designing the frameworks for different IR tasks based on their degradation process, which can be roughly divided into two categories, CNN-based framework [10, 12, 77], and Transformer-based framework [8, 26, 34, 69]. Despite that, the above works only explore how to improve the ability of inductive bias toward specific degradation, which lacks enough generalization capability. To improve the model’s robustness, some works seek to incorporate the domain translation [14, 37, 50] or distortion-adaptive learning [62] into image restoration. In contrast, we introduce causal learning [18] to image restoration. We answer the reason for the bad robustness of the restoration network and propose *distortion-invariant representation learning from a causality perspective*.

2.2. Causal Inference

Causal Inference is proposed to eliminate the harmful bias of confounders and discover the causal relationship between multiple variables [18]. A *do* operation is implemented with adjustment criteria, *e.g.*, front-door or back-door, to estimate the causal effects [46]. In recent years, deep learning has boosted the vast development of a series of intelligent tasks, *e.g.*, image classification [11, 13, 36], segmentation [20, 49], detection [6, 32], low-level processing [8, 53]. However, prominent works focus on fitting the *correlation* between inputs and their outputs while ignoring the *causation*. Due to the existence of confounders, the networks are easy to capture the spurious correlation between inputs and their outputs. For instance, if *most lions lie in the grass* in the training data, the model inevitably mistakes the grass for a lion. To get rid of the harmful bias of confounders, some studies seek to incorporate causal inference into deep learning. [56, 68] model the interventions of confounders from the feature perspective [65] integrate the front-door criterion to vision-language task from the attention perspective. To improve the generalization capability, [31, 38, 39, 67] introduce the causal learning to domain adaptation/generalization. However, the above causality-inspired methods merely focus on the high-level tasks. In this paper, for the first time, we investigate the causality-based image restoration, which aims to improve the generalization capability of restoration networks on different distortion types and degrees.

3. Methods

3.1. A Causal View for Image Restoration

Image restoration aims to restore the distorted images, of which the degradation process can be represented as a function $I_d = g(I_c, D)$. Here, I_c, I_d, D denotes the clean, distorted images, and distortions, respectively. A restoration network f is trained with the loss function to minimize the difference between its ideal reconstructed images I_o and the original clean image I_c . We model this whole process with a causal structure graph as shown in Fig. 2. Here, $D \rightarrow I_d \leftarrow I_c$ denotes the degradation process of $I_d = g(I_c, D)$. $I_c \rightarrow I_o$ denotes I_o is learned with the supervision of I_c by maximizing the probability of $P(I_c|I_o)$. In addition, $D \rightarrow I_o$ refers to the knowledge learned from D to I_o . $I_d \rightarrow I_o$ means the restoration process with restoration network f .

From the causality perspective, the causal representation of image restoration requires that the restoration network f obtains the causal relationship between $I_d \rightarrow I_o$ (*i.e.*, $P(I_o|do(I_d))$). However, there are two extra paths $I_d \leftarrow D \rightarrow I_o$ and $I_d \leftarrow I_c \rightarrow I_o$ introducing the spurious correlation to I_d and I_o , where I_c and D are confounders in causality. Importantly, the I_c are commonly diverse in the datasets and bring more vivid textures to reconstructed image I_o , which is a favorable confounder. We do not take into account of the confounder I_c in our paper.

We aim to improve the robustness of the restoration network to unseen or unknown distortions, which are inhibited by the bad confounding effects from confounders D . But, *how do the confounders D limit the generalization capability of the restoration network?* As shown in Fig. 2, the existing of $I_d \leftarrow D \rightarrow I_o$ causes the conditional probability $P(I_o|I_d)$ learned by restoration network f is also condition on distortions D , *i.e.*, the fitting conditional probability of f is in fact as $P(I_o|I_d, D)$. Consequently, the restoration network f is not robust to different distortions due to that it is not independent of different distortions D .

A robust restoration network f should be independent of different distortions (*i.e.*, $D \perp\!\!\!\perp I_o|I_d$). To achieve this, we adopt the back-door criterion in causal inference to realize distortion-invariant learning (DIL). We formulate the back-door criterion in image restoration as Equ. 1.

$$P(I_o|do(I_d)) = \sum_{d_i \in D} P(I_o|I_d, d_i)P(d_i), P(d_i) = \frac{1}{n}, \quad (1)$$

where the causal conditional probability $P(I_o|do(I_d))$ is the optimization direction for restoration network f towards distortion invariant learning. To simplify the optimization, we set the probability of each distortion d_i as $1/n$, where n is the number of distortion types and degrees that existed in confounders. From Equ. 1, two crucial challenges for achieving it arise. 1) *How to construct the virtual confounders (*i.e.*, different distortion types or degrees)? since*

collecting different real distorted images with the same contents are nontrivial in the real world. 2) How to instantiate the intervention of different distortions to the reconstruction process (i.e., the $P(I_o|I_d, d_i)$) in image restoration. We achieve this through counterfactual distortion augmentation and distortion-invariant representation learning as described in the following sections.

3.2. Counterfactual Distortion Augmentation

To learn the distortion-invariant representation for the restoration network, it is vital to construct the distortion set D (i.e., confounders). For instance, if we expect the restoration network to have the generalization capability for different distortion degrees, we require to construct the distortion set D with the distortions at different levels. Similarly, we can increase the generalization capability of the restoration network for unknown distortion types by constructing the D with different but related distortion types. Furthermore, to avoid the effects of different image contents, it is better for each clean image to have corresponding distorted images with various distortion types or degrees in D . However, it is non-trivial to collect datasets that satisfy the above principles in the real world, which is labor-intensive and arduous.

In this paper, we construct the distortion set D with synthesized distortions, which we can call them virtual confounders in causality. Concretely, we collected a series of high-quality images I_c , and generated the distorted images by modifying the degradation process as $I_d = g(I_c, d_i), d_i \in D$. We can also prove the rightness of the above distortion augmentation from the counterfactuals in causality [18], where we answer the counterfactual question that “if D is d_i , what the I_d would be with I_c invariant?”. The proof can be found in the **Supplementary**.

3.3. Distortion-invariant Representation Learning

After constructing the virtual confounders/distortions set $D = \{d_i | 1 \leq i \leq n\}$. We are able to achieve the distortion-invariant representation learning by implementing the back-door criterion as Eq. 1 for image restoration. Let us first introduce the relationship between the probability $P(I_o|I_d)$ and the commonly-used training paradigm ERM (empirical risk minimization). In image restoration, an ideal reconstruction I_o is expected to learn by maximizing the condition probability $P(I_o|I_d)$ with loss function as $\mathcal{L}(f_\theta(I_d), I_c)$, where f_θ is the restoration network with the parameters θ and L denotes the loss function, such as the commonly-used \mathcal{L}_1 or \mathcal{L}_2 loss. The ERM is used to optimize the network f_θ (with parameters denoted by θ) by minimizing the loss function overall training dataset $\mathcal{D} = \{I_d, I_c | d \in D\}$ as:

$$\theta^* = \arg \min_{\theta} \mathbb{E}_{(I_d, I_c) \sim \mathcal{D}} [\mathcal{L}(f_\theta(I_d), I_c)], \quad (2)$$

where θ^* enables the restoration network f to maximize the $P(I_o|I_d) \approx P(I_c|I_d)$. However, the above training process also leads the $P(I_o|I_d)$ to be not independent to the distortions $d \in D$ in the training dataset \mathcal{D} , which eliminate the generalization ability of f on the out-of-distribution distortions (i.e., when $d \notin D$). To achieve the distortion-invariant representation learning, we aim to maximize the causal conditional probability $P(I_o|do(I_d))$ as instead of $P(I_o|I_d)$. The key challenge stems from how to model the conditional probability $P(I_o|I_d, d_i)$ in Eq. 1 (i.e., how to model the intervention from the distortion $d_i \in D$ for the restoration process $P(I_o|I_d)$).

In this paper, we propose to model the intervention from $d_i \in D$ to the restoration process (i.e., $P(I_o|I_d, d_i)$) through the optimization of the network parameters θ . From the above analysis, we know that the restoration network f_θ trained with ERM on the paired training data (I_{d_i}, I_c) is condition on the distortion d_i . This inspires us to instantiate the intervention of different distortion types or degrees $d_i \in D$ through updating the model parameter θ to ϕ_{d_i} based on ERM with the training distorted-and-clean image pairs (I_{d_i}, I_c) as:

$$\phi_{d_i} = \theta - \alpha \nabla_{\theta} \mathcal{L}(f_{\theta}(I_{d_i}), I_c), \quad (3)$$

where ϕ_{d_i} denotes the parameters of the restoration network after one-step update, which is conditioned on the confounder d_i . Consequently, the maximum of the conditional probability $P(I_o|I_d, d_i)$ can be obtained by minimizing the loss $\mathcal{L}(f_{\phi_{d_i}}(I_d), I_c)$. The optimization direction toward maximizing the causal condition probability $P(I_o|do(I_d))$ in Eq. 1 can be derived as:

$$\theta^* = \arg \min_{\theta} \mathbb{E}_{(I_d, I_c) \sim \mathcal{D}} \left[\sum_{d_i \in D} \mathcal{L}(f_{\phi_{d_i}}(I_d), I_c) \right], \quad (4)$$

where D denotes the confounder set which contains n distortion degrees or types. Based on the above optimization objective, we learn distortion-invariant representation learning from a causality perspective.

3.4. Implementations of DIL from Meta-Learning

An interesting finding is that the derived optimization direction of DIL from causality perspective in Eq. 8 is consistent with one typical meta-learning strategy termed as MAML [15], even they have different purposes. MAML aims to enable the fast adaptation capability of a network for few-shot tasks, while ours aims to improve the generalization capability of the restoration network. We facilitate our DIL in image restoration based on this meta-learning strategy.

However, it is arduous to directly incorporate the optimization direction of Eq. 8 into the practical training process, which is computationally prohibitive. The reason

Table 1. Quantitative comparison for image denoising on several benchmark datasets. Results are tested on three different unseen distortion degrees in terms of PSNR/SSIM on RGB channel. Best performances are **bolded**.

Datasets	Levels	Methods				
		ERM	DIL _{sf}	DIL _{pf}	DIL _{ss}	DIL _{ps}
CBSD68 [40]	30 (<i>unseen</i>)	24.90/0.581	30.29 ^(5.39↑) / 0.866	29.92 ^(5.02↑) /0.858	27.48 ^(2.58↑) /0.809	29.14 ^(4.24↑) /0.802
	40 (<i>unseen</i>)	21.12/0.400	28.35 ^(7.23↑) / 0.825	28.10 ^(6.98↑) /0.812	25.90 ^(4.78↑) /0.746	25.74 ^(4.62↑) /0.629
	50 (<i>unseen</i>)	18.96/0.307	26.64 ^(7.68↑) / 0.779	26.61 ^(7.65↑) /0.766	24.63 ^(5.67↑) /0.686	23.34 ^(4.38↑) /0.501
Kodak24 [16]	30 (<i>unseen</i>)	25.12/0.533	31.39 ^(6.27↑) / 0.867	30.87 ^(5.75↑) /0.858	27.92 ^(2.80↑) /0.801	29.86 ^(4.74↑) /0.782
	40 (<i>unseen</i>)	21.22/0.352	29.49 ^(8.27↑) / 0.831	29.15 ^(7.93↑) /0.817	26.46 ^(5.24↑) /0.738	26.13 ^(4.91↑) /0.588
	50 (<i>unseen</i>)	19.02/0.263	27.76 ^(8.74↑) / 0.788	27.67 ^(8.65↑) /0.775	25.24 ^(6.22↑) /0.677	23.60 ^(4.58↑) /0.457
McMaster [75]	30 (<i>unseen</i>)	25.65/0.569	31.70 ^(6.05↑) / 0.873	31.04 ^(5.39↑) /0.853	28.15 ^(2.50↑) /0.794	30.09 ^(4.44↑) /0.800
	40 (<i>unseen</i>)	21.73/0.373	29.81 ^(8.08↑) / 0.831	29.07 ^(7.34↑) /0.802	26.59 ^(4.86↑) /0.728	26.24 ^(4.51↑) /0.605
	50 (<i>unseen</i>)	19.47/0.278	28.02 ^(8.55↑) / 0.783	27.31 ^(7.84↑) /0.749	25.20 ^(5.73↑) /0.664	23.60 ^(4.13↑) /0.466
Urban100 [22]	30 (<i>unseen</i>)	25.46/0.648	30.93 ^(5.47↑) / 0.898	30.26 ^(4.80↑) /0.884	26.95 ^(1.49↑) /0.825	29.73 ^(4.27↑) /0.841
	40 (<i>unseen</i>)	21.53/0.479	28.82 ^(7.29↑) / 0.866	28.32 ^(6.79↑) /0.848	25.26 ^(3.73↑) /0.767	26.25 ^(4.72↑) /0.691
	50 (<i>unseen</i>)	19.28/0.389	26.88 ^(7.60↑) / 0.829	26.63 ^(7.35↑) /0.811	23.85 ^(4.57↑) /0.710	23.71 ^(4.43↑) /0.575
Manga109 [41]	30 (<i>unseen</i>)	26.62/0.653	31.97 ^(5.35↑) / 0.910	31.14 ^(4.52↑) /0.901	26.02 ^(-0.6↑) /0.833	31.05 ^(4.43↑) /0.858
	40 (<i>unseen</i>)	22.34/0.442	29.02 ^(6.68↑) / 0.888	28.53 ^(6.19↑) /0.875	24.31 ^(1.97↑) /0.784	27.29 ^(4.95↑) /0.704
	50 (<i>unseen</i>)	19.95/0.342	26.52 ^(6.57↑) / 0.860	26.34 ^(6.39↑) /0.846	22.82 ^(2.87↑) /0.734	24.47 ^(4.52↑) /0.564

is that it requires multiple gradient computing and updating, which is expensive, especially for the pixel-wise image restoration. To simplify this process, we utilize the Taylor expansion and inverse expansion to derive Eq. 8 as:

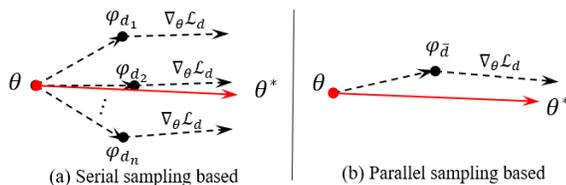


Figure 3. The comparison of serial sampling and parallel sampling.

$$\theta^* = \arg \min_{\theta} \mathbb{E}_{(I_d, I_c) \sim \mathcal{D}} [\mathcal{L}(f_{\phi_{\bar{d}}}(I_d), I_c)],$$

$$\text{where } \phi_{\bar{d}} = \theta - \alpha \nabla_{\theta} \sum_{d_i \in \mathcal{D}} \frac{1}{n} \mathcal{L}(f_{\theta}(I_{d_i}), I_c), \quad (5)$$

where $\phi_{\bar{d}}$ denotes the parameters of restoration network f that is virtually updated with loss function with samples overall all distortions $\mathcal{D} = \{d_i\}, 1 \leq i \leq n$. We define it as *parallel sampling* for DIL, which reduces the complex training process of **DIL** to two steps. In this paper, we call the original sampling strategy as *serial sampling*. The comparison between *serial sampling* and *parallel sampling* are shown in Fig. 3. The detailed derivation for Eq. 5 are described in the **Supplementary**.

We also investigate two different gradient updating strategy for DIL. From Eq. 8 and Eq. 5, we can observe that they require the second-order gradient since the gradient is computed with two-step forward through ϕ_{d_i} , which is shown in Fig. 3. To simplify it, Reptile [44] proposes an alternative strategy (*i.e.*, approximating the second-order gradient by the sequential parameter updating with one-order gradient. The optimization direction (*i.e.*, gradient) is computed with

the deviation between the initial and last-step parameters. We integrate it into our DIL and call it first-order optimization. In contrast, the original optimization in Eq. 5 is termed second-order optimization. In summary, we propose four variants for DIL following the above two strategies. DIL_{sf} adopts the serial sampling and first-order gradient optimization. DIL_{pf} utilizes the parallel sampling and first-order optimization. DIL_{ss}/DIL_{ps} exploits the second-order optimization and serial/parallel sampling.

4. Experiments

In this section, we first describe the implementation details. Then, we validate the effectiveness of our DIL from two typical out-of-distribution settings, *i.e.*, Cross Distortion Degrees, and Cross Distortion Types. Particularly, for cross-distortion degrees, we train the restoration network with seen distortion degrees while testing it with unseen distortion degrees. For cross-distortion types, the restoration network is trained with synthesized distortions and validated on the corresponding real-world or other distortions.

4.1. Implementation

We adopt the typical RRDB [58] as our image restoration backbone, which has demonstrated remarkable performances towards various low-level image tasks [54, 57]. All the experiments are done with four NVIDIA 2080Ti GPUs. Adam optimizer is adopted to optimize network parameters in both ERM and **DIL** training paradigms. More details are given in the **Supplementary**.

4.2. Cross Distortion Degrees

Results on Image Denoising. For image denoising, the training data are composed of distorted images with noise levels [5, 10, 15, 20] and their corresponding clean images.

Table 2. Quantitative comparison for image deblurring on several benchmark datasets. Results are tested on the five unseen blur degrees [4.2, 4.4, 4.6, 4.8, 5.0] in terms of PSNR/SSIM on RGB channel.

Datasets	Methods	Levels				
		4.2 (<i>unseen</i>)	4.4 (<i>unseen</i>)	4.6 (<i>unseen</i>)	4.8 (<i>unseen</i>)	5.0 (<i>unseen</i>)
Set5 [4]	ERM	29.31/0.844	26.55/0.776	24.43/0.709	22.96/0.648	22.00/0.602
	DIL	29.58(0.27↑)/0.848	27.52(0.97↑)/0.802	25.66(1.23↑)/0.751	24.38(1.42↑)/0.708	23.46(1.46↑)/0.671
Set14 [71]	ERM	27.22/0.781	24.93/0.726	23.16/0.671	21.89/0.624	20.88/0.583
	DIL	27.24(0.02↑)/0.778	25.78(0.85↑)/0.746	24.35(1.19↑)/0.708	23.23(1.34↑)/0.672	22.37(1.49↑)/0.640
BSD100 [40]	ERM	27.20/0.784	25.17/0.732	23.50/0.682	22.24/0.639	21.28/0.602
	DIL	27.37(0.17↑)/0.781	26.16(0.99↑)/0.753	24.91(1.41↑)/0.719	23.86(1.62↑)/0.686	23.02(1.74↑)/0.658
Urban100 [22]	ERM	24.95/0.797	22.41/0.723	20.59/0.657	19.33/0.606	18.40/0.565
	DIL	24.97(0.02↑)/0.793	23.26(0.85↑)/0.743	21.76(1.17↑)/0.693	20.70(1.37↑)/0.651	19.92(1.52↑)/0.618
Manga109 [41]	ERM	28.16/0.865	23.96/0.791	21.21/0.713	19.63/0.652	18.63/0.606
	DIL	28.09(-0.07↓)/0.867	25.41(1.45↑)/0.822	23.15(1.94↑)/0.771	21.69(2.06↑)/0.726	20.72(2.09↑)/0.691

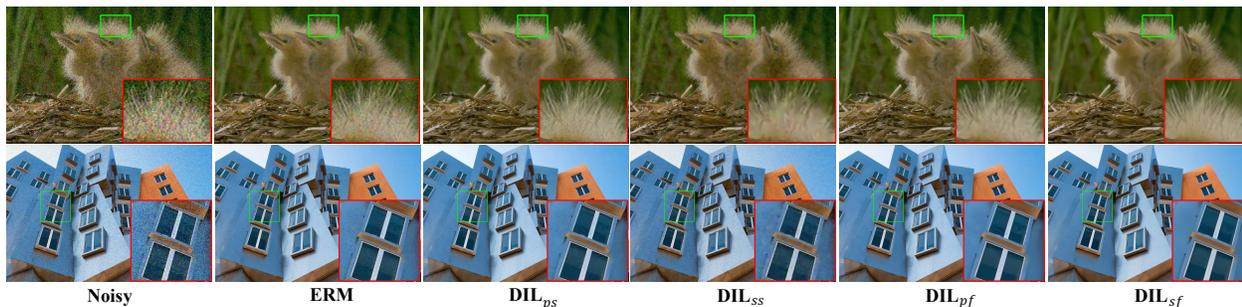


Figure 4. Visual comparison of the commonly-used ERM and our proposed four variants of DIL with the unseen noise level 30.

After training the restoration network, we validate it on the test datasets with unseen noise degrees, including [30, 40, 50]. We compare the empirical risk minimization (ERM) and four variants of our proposed DIL, *i.e.*, DIL_{sf} , DIL_{pf} , DIL_{ss} , and DIL_{ps} , respectively.

Table 3. Quantitative comparison for hybrid distortion removal. Results are tested on three different distortion levels in terms of PSNR/SSIM on Y channel.

Datasets	Methods	Distortion level		
		Mild (<i>unseen</i>)	Moderate (<i>unseen</i>)	Severe (<i>seen</i>)
BSD100 [40]	ERM	25.31/0.687	24.62/0.642	25.27/0.617
	DIL	26.37/0.691	25.23/0.645	25.22/0.613
Urban100 [22]	ERM	23.97/0.736	22.51/0.674	23.38/0.655
	DIL	25.00/0.747	23.13/0.682	23.20/0.645
Manga109 [41]	ERM	27.43/0.863	24.85/0.808	26.50/0.815
	DIL	28.41/0.868	25.30/0.810	26.19/0.766
DIV2K [2]	ERM	26.19/0.766	25.94/0.744	27.42/0.742
	DIL	27.84/0.785	26.89/0.756	27.38/0.737

The experimental results are shown in Table 1. We can observe that all four variants of DIL achieve great generalization ability on multiple unseen noise levels compared with commonly-used empirical risk minimization (ERM). On several typical scenarios, including natural images (*i.e.*, CBSD68 [40], Kodak24 [16], McMaster [75]), building images (Urban100 [22]), cartoon images (*i.e.*, Manga109 [41]), our DIL even outperforms the ERM by

a promising/amazing gain of 8.74 dB at most. Moreover, with the increase of the distribution gap between training and testing data, ours can achieve larger improvements for ERM. Furthermore, for cross distortion degree, DIL_{sf} shows the best generalization capability compared with the other three variants by serial sampling and first-order optimization. We also visualize the reconstructed images of the above methods in Fig. 4. For the unseen distortion degree ($\sigma = 30$), the ERM cannot remove the noise well and the reconstructed image also contains obvious noise distortion. However, our DIL_{sf} enables the restoration network to recover more vivid and clean images from the unseen noise degrees, which validates the correctness and effectiveness of our proposed DIL.

Results on Image Deblurring. We also validate the generalization capability of our DIL on the challenging image deblurring. Under this scenarios, we train the restoration network with our proposed DIL with the gaussian blurring level [1.0, 2.0, 3.0, 4.0], and validate its generalization capability on the more severe and difficult blurring levels, including 4.2, 4.4, 4.6, 4.8, and 5.0.

As shown in Table 2, we validate our DIL on five benchmark datasets, including Set5 [4], Set14 [71], BSD100 [40], Urban100 [22], and Manga109 [41]. With the increase of blurring level, the restoration network trained with ERM suffers from a severe performance drop, since the unseen blurring levels are far away from the blurring levels used for training. But our DIL can improve ERM on each unseen

Table 4. Quantitative results of network generalization capability on real image denoising and synthetic image deraining tasks. Results are tested on Y channel in terms of PSNR/SSIM, except for DND where we obtain our results from official online benchmark.

Methods	Datasets (Real Denoising)		Datasets (Deraining)		
	SIDD [1]	DND [47]	Rain100L [64]	Rain12 [33]	Rain800 [73]
ERM	38.90/0.9379	38.67/0.9549	27.61/0.8577	31.44/0.8947	23.36/0.8199
DIL _{sf}	39.96 _(1.06↑) /0.9410	39.16 _(0.49↑) /0.9531	28.15 _(0.54↑) /0.8679	32.43 _(0.99↑) /0.9163	23.41 _(0.05↑) /0.8261
DIL _{ps}	39.92 _(1.02↑) /0.9385	39.03 _(0.36↑) /0.9553	28.37 _(0.76↑) /0.8739	33.07 _(1.63↑) /0.9266	23.52 _(0.16↑) /0.8281



Figure 5. Visual comparison of the commonly-used ERM and our proposed DIL for unseen hybrid-distorted (mild) image restoration.

blurring level for five datasets. In particular, we achieve the gain of 2.09 dB for the cartoon scene Manga109 [41] on the blurring level 5.0.

Results on Hybrid-distorted Image Restoration. Except for the above single distortion, we also explore the generalization capability of our DIL on hybrid-distorted image restoration. Following [28], the hybrid distorted images are degraded with blur, noise, and Jpeg compression in a sequence manner. Based on the distortion degree, it can be divided into three levels from low to high, *i.e.*, mild, moderate, and severe. In this setting, the restoration network is trained with severe hybrid distortions and validated on the mild and moderate levels.

As shown in Table 3, our DIL achieves an average gain of 1.05 dB, and 0.66 dB on the mild-level, and moderate-level hybrid distortions than ERM, which has a large distribution gap with severe-level hybrid distortions. We can also notice that with the increase of the distribution gap, ours can preserve more performances on the restoration of the out-of-distribution distortions. We also conduct the subjective comparison of our methods with the commonly-used ERM in Fig. 5. We can observe that the restoration network trained with ERM suffers from new artifacts for unseen hybrid-distorted images. But our DIL can eliminate the artifacts well and generate more promising results.

4.3. Cross Distortion Types

In this section, we investigate the effects of our proposed DIL on the cross-distortion type setting, which is more challenging than the cross-degree setting.

Results on Real Image Super-resolution Real Image Super-resolution (RealSR) has attracted great attention since it is urgently required in real life, where the distorted image contains complex hybrid distortions, such as blurring, low resolution, noise, etc. However, the distorted/clean pairs for RealSR are hard to be collected. Simulating distortions like Real-world distortion has been a popular solution for RealSR [57, 74]. In this paper, we fol-

low the Real-ESRGAN [57] and utilize its proposed RealSR distortion simulating to generate image pairs as training datasets. Then we test the restoration network on the out-of-distribution datasets, RealSR V3 [5], DRealSR [61], which are two commonly-used datasets for RealSR evaluation.

Table 5. Quantitative results of the network generalization capability on RealSR tasks. Results are tested on the Y channel in terms of PSNR/SSIM.

Methods	Datasets	
	RealSR V3 [5] (unseen)	DRealSR [61] (unseen)
Real-ESRNet [57]	26.19/0.7989	28.22/0.8470
BSRNet [74]	27.46/0.8082	29.45/0.8579
ERM	27.65/0.8098	29.73/0.8628
DIL _{sf}	27.94 _(0.29↑) /0.8098	29.99 _(0.26↑) /0.8648
DIL _{ps}	28.12 _(0.47↑) /0.8067	30.58 _(0.85↑) /0.8712

Table 6. Quantitative results of our DIL on different backbones. Results are tested on the unseen noise level 30 in terms of PSNR/SSIM.

Models	Methods	Datasets		
		CBSD68 [40]	Kodak24 [16]	Urban100 [22]
RRDB	ERM	24.90/0.581	25.12/0.533	25.46/0.648
	DIL	30.28/0.866	31.39/0.867	30.93/0.898
SwinIR	ERM	24.22/0.551	24.22/0.493	24.73/0.618
	DIL	29.08/0.798	29.71/0.774	29.72/0.834

We show the experimental results on RealSR in Table. 5. Without access to any training samples in RealSR V3, DRealSR, our DIL_{sf} can outperform the ERM by 0.29dB on RealSR V3 [5] and 0.26dB on DRealSR dataset [61]. Particularly, we notice that DIL_{ps} is more suitable for cross-distortion type scenarios than DIL_{sf}, which exceeds the ERM by a 0.47dB on RealSR V3, and 0.85dB on DRealSR dataset. The reason for that we guess is that DIL_{ps} is more capable of improving the generalization for the large distribution gap in image restoration. We also visualize the comparison corresponding to the subjective quality for different methods. As shown in Fig. 6, Real-ESRNet [57] and BSR-

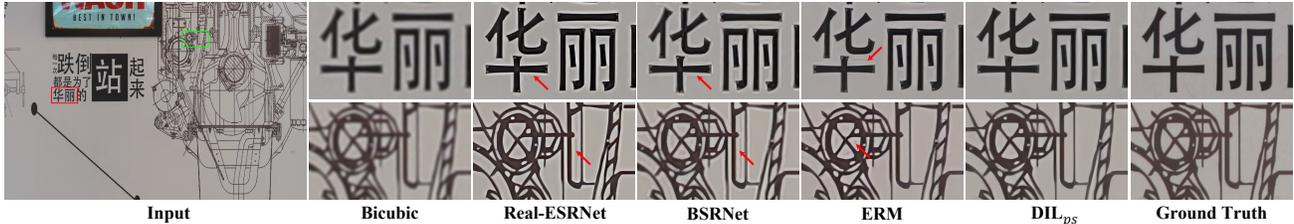


Figure 6. Visual comparison with state-of-the-art methods on DRealSR [61].

Net [74] cause the overshooting at the edge of the text. But our DIL_{ps} can eliminate the artifacts and achieve a high-quality restoration

Table 7. Quantitative comparison between different distortion augmentation methods. D_1 and D_2 are the first order distortion and the second order distortion derived from [57] respectively. Results are tested on RealSR datasets in terms of PSNR/SSIM.

Augmentation	Methods	Datasets	
		RealSR V3 [5]	DrealSR [61]
D_1	ERM	27.65/0.8098	29.73/0.8628
	DIL	27.94/0.8098	29.99/0.8648
D_2	ERM	27.39/0.8077	29.41/0.8591
	DIL	27.65/0.8027	29.85/0.8677

Results on Real Image Denoising. We also study the generalization capability of our training paradigm DIL on the Real Image Denoising task. Concretely, we select four synthesized distortions based on four categories of color space among camera ISP process [19], and generate training image pairs from DF2K [2, 51] in an online manner. Then we verify its generalization on the commonly-used Real Denoising dataset SIDD [1] and DND [47]. As Table 4 illustrated, our DIL_{ps} achieves the PSNR of 39.92 dB, which outperforms the ERM by 1.02dB, which is almost the same with DIL_{sf} .

Results on Image Deraining. As an extension experiment, we introduce our DIL to the experiments of image deraining task. Particularly, the raining types and degrees between different datasets are severely different in image deraining. Here, we optimize the restoration network with three image deraining datasets, including DID-MDN [72], Rain14000 [17], and Heavy Rain Dataset [27]. Then we validate the generalization capability of the restoration network on three unseen deraining datasets, *i.e.*, Rain100L [64], Rain12 [33], and Rain800 [73]. We report the experimental results in Table 4. Our DIL (DIL_{ps}) enables the restoration network to have a better generalization capability than ERM, which obtains a gain of 0.76dB on Rain100L [64] and 1.63dB on Rain12 [33] dataset.

4.4. Ablation Studies

Impact of different restoration networks. We demonstrate the effectiveness of DIL across different network backbones. In addition to the convolution-based RRDB [58] network, we also incorporate our DIL into the

transformer-based SwinIR [34]. The performances are reported in Table 6, which reveals that our DIL can also improve the generalization capability of Transformer-based backbones. This study reveals our DIL is a general training paradigm for different backbones.

Effects of different variants for DIL As shown in Table 1, and 4, we can observe that DIL_{sf} is more proper for cross-distortion degrees. But for cross-distortion types, DIL_{ps} achieves better performance for RealSR and Image Deraining. It is noteworthy that the distribution gap of different distortion types is larger than different degrees. The first-order optimization is more stable but lacks enough capability for a severe distribution gap compared to second-order optimization. But all of them are competent in improving the generalization capability.

5. Discussion on Limitations

The performance on training data. We also report the performance of our DIL on the seen training data in Table 3. It can be seen that our DIL will cause a slight performance drop but the generalization capability is improved obviously. The reason for that is our DIL implements distortion invariant representation learning, which prevents the restoration network from over-fitting to the training data.

The impact of different distortion augmentation. As shown in Table 7, despite that our DIL achieves the improvement of the generalization capability. The final generalization performance is still related to the distortion augmentation strategy. It is vital to find a universal distortion augmentation strategy, which requires more exploration. We believe it will be a potential/important direction to improve the generalization ability of the restoration network.

6. Conclusion

In this paper, we propose a novel *distortion invariant representation learning (DIL)* training paradigm for image restoration from the causality perspective. In particular, we provide a causal view of the image restoration process, and clarify why the restoration network lacks the generalization capability for different degradations. Based on that, we treat the distortion types and degrees as confounders, of which the confounding effects can be removed with our proposed **DIL**. Concretely, we produce the spurious confounders by simulating the different distortion types and degrees. Then, an instantiation of the back-door criterion in causality is in-

roduced from the optimization perspective, which enables the restoration network to remove the harmful bias from different degradations. Extensive experiments on the settings, cross distortion degrees, and cross distortion types, have demonstrated that our **DIL** improves the generalization capability of the restoration network effectively.

Acknowledgements

This work was supported in part by NSFC under Grant U1908209, 62021001, and ZJNSFC under Grant LQ23F010008.

References

- [1] Abdelrahman Abdelhamed, Stephen Lin, and Michael S Brown. A high-quality denoising dataset for smartphone cameras. In *Proceedings of the IEEE Conference on Computer Vision and Pattern Recognition*, pages 1692–1700, 2018. [7](#), [8](#), [16](#), [18](#)
- [2] Eirikur Agustsson and Radu Timofte. Ntire 2017 challenge on single image super-resolution: Dataset and study. In *Proceedings of the IEEE conference on computer vision and pattern recognition workshops*, pages 126–135, 2017. [2](#), [6](#), [8](#), [15](#), [16](#)
- [3] Saeed Anwar and Nick Barnes. Real image denoising with feature attention. In *Proceedings of the IEEE/CVF international conference on computer vision*, pages 3155–3164, 2019. [1](#), [3](#)
- [4] Marco Bevilacqua, Aline Roumy, Christine Guillemot, and Marie Line Alberi-Morel. Low-complexity single-image super-resolution based on nonnegative neighbor embedding. 2012. [6](#)
- [5] Jianrui Cai, Hui Zeng, Hongwei Yong, Zisheng Cao, and Lei Zhang. Toward real-world single image super-resolution: A new benchmark and a new model. In *Proceedings of the IEEE/CVF International Conference on Computer Vision*, pages 3086–3095, 2019. [7](#), [8](#), [16](#)
- [6] Nicolas Carion, Francisco Massa, Gabriel Synnaeve, Nicolas Usunier, Alexander Kirillov, and Sergey Zagoruyko. End-to-end object detection with transformers. In *European conference on computer vision*, pages 213–229. Springer, 2020. [3](#)
- [7] Pierre Charbonnier, Laure Blanc-Feraud, Gilles Aubert, and Michel Barlaud. Two deterministic half-quadratic regularization algorithms for computed imaging. In *Proceedings of 1st International Conference on Image Processing*, volume 2, pages 168–172. IEEE, 1994. [15](#)
- [8] Hanting Chen, Yunhe Wang, Tianyu Guo, Chang Xu, Yiping Deng, Zhenhua Liu, Siwei Ma, Chunjing Xu, Chao Xu, and Wen Gao. Pre-trained image processing transformer. In *Proceedings of the IEEE/CVF Conference on Computer Vision and Pattern Recognition*, pages 12299–12310, 2021. [1](#), [3](#)
- [9] Yinbo Chen, Sifei Liu, and Xiaolong Wang. Learning continuous image representation with local implicit image function. In *Proceedings of the IEEE/CVF conference on computer vision and pattern recognition*, pages 8628–8638, 2021. [1](#)
- [10] Tao Dai, Jianrui Cai, Yongbing Zhang, Shu-Tao Xia, and Lei Zhang. Second-order attention network for single image super-resolution. In *Proceedings of the IEEE/CVF conference on computer vision and pattern recognition*, pages 11065–11074, 2019. [3](#)
- [11] Jia Deng, Wei Dong, Richard Socher, Li-Jia Li, Kai Li, and Li Fei-Fei. Imagenet: A large-scale hierarchical image database. In *2009 IEEE conference on computer vision and pattern recognition*, pages 248–255. Ieee, 2009. [3](#)
- [12] Chao Dong, Chen Change Loy, Kaiming He, and Xiaoou Tang. Image super-resolution using deep convolutional networks. *IEEE transactions on pattern analysis and machine intelligence*, 38(2):295–307, 2015. [1](#), [3](#)
- [13] Alexey Dosovitskiy, Lucas Beyer, Alexander Kolesnikov, Dirk Weissenborn, Xiaohua Zhai, Thomas Unterthiner, Mostafa Dehghani, Matthias Minderer, Georg Heigold, Sylvain Gelly, et al. An image is worth 16x16 words: Transformers for image recognition at scale. *arXiv preprint arXiv:2010.11929*, 2020. [1](#), [3](#)
- [14] Wenchao Du, Hu Chen, and Hongyu Yang. Learning invariant representation for unsupervised image restoration. In *Proceedings of the IEEE/CVF conference on computer vision and pattern recognition*, pages 14483–14492, 2020. [2](#), [3](#)
- [15] Chelsea Finn, Pieter Abbeel, and Sergey Levine. Model-agnostic meta-learning for fast adaptation of deep networks. In *International conference on machine learning*, pages 1126–1135. PMLR, 2017. [4](#)
- [16] Rich Franzen. Kodak lossless true color image suite. *source: http://r0k.us/graphics/kodak*, 4(2), 1999. [5](#), [6](#), [7](#)
- [17] Xueyang Fu, Jiabin Huang, Delu Zeng, Yue Huang, Xinghao Ding, and John Paisley. Removing rain from single images via a deep detail network. In *Proceedings of the IEEE conference on computer vision and pattern recognition*, pages 3855–3863, 2017. [8](#), [16](#)
- [18] Madelyn Glymour, Judea Pearl, and Nicholas P Jewell. *Causal inference in statistics: A primer*. John Wiley & Sons, 2016. [2](#), [3](#), [4](#), [13](#)
- [19] Shi Guo, Zifei Yan, Kai Zhang, Wangmeng Zuo, and Lei Zhang. Toward convolutional blind denoising of real photographs. In *Proceedings of the IEEE/CVF conference on computer vision and pattern recognition*, pages 1712–1722, 2019. [8](#), [16](#)
- [20] Kaiming He, Georgia Gkioxari, Piotr Dollár, and Ross Girshick. Mask r-cnn. In *Proceedings of the IEEE international conference on computer vision*, pages 2961–2969, 2017. [3](#)
- [21] Kaiming He, Xiangyu Zhang, Shaoqing Ren, and Jian Sun. Deep residual learning for image recognition. In *Proceedings of the IEEE conference on computer vision and pattern recognition*, pages 770–778, 2016. [1](#)
- [22] Jia-Bin Huang, Abhishek Singh, and Narendra Ahuja. Single image super-resolution from transformed self-exemplars. In *Proceedings of the IEEE conference on computer vision and pattern recognition*, pages 5197–5206, 2015. [5](#), [6](#), [7](#)
- [23] Kui Jiang, Zhongyuan Wang, Peng Yi, Chen Chen, Baojin Huang, Yimin Luo, Jiayi Ma, and Junjun Jiang. Multi-scale progressive fusion network for single image deraining. In *Proceedings of the IEEE/CVF conference on computer vision and pattern recognition*, pages 8346–8355, 2020. [16](#)

- [24] Xin Jin, Li Zhang, Chaowei Shan, Xin Li, and Zhibo Chen. Dual prior learning for blind and blended image restoration. *IEEE Transactions on Image Processing*, 31:1042–1056, 2021. [3](#)
- [25] Seunghwan Lee, Donghyeon Cho, Jiwon Kim, and Tae Hyun Kim. Self-supervised fast adaptation for denoising via meta-learning. *arXiv preprint arXiv:2001.02899*, 2020. [1](#)
- [26] Bingchen Li, Xin Li, Yiting Lu, Sen Liu, Ruoyu Feng, and Zhibo Chen. Hst: Hierarchical swin transformer for compressed image super-resolution. *arXiv preprint arXiv:2208.09885*, 2022. [1](#), [3](#)
- [27] Ruoteng Li, Loong-Fah Cheong, and Robby T Tan. Heavy rain image restoration: Integrating physics model and conditional adversarial learning. In *Proceedings of the IEEE/CVF Conference on Computer Vision and Pattern Recognition*, pages 1633–1642, 2019. [8](#), [16](#)
- [28] Xin Li, Xin Jin, Jianxin Lin, Sen Liu, Yaojun Wu, Tao Yu, Wei Zhou, and Zhibo Chen. Learning disentangled feature representation for hybrid-distorted image restoration. In *European Conference on Computer Vision*, pages 313–329. Springer, 2020. [3](#), [7](#), [16](#)
- [29] Xin Li, Xin Jin, Tao Yu, Simeng Sun, Yingxue Pang, Zhizheng Zhang, and Zhibo Chen. Learning omni-frequency region-adaptive representations for real image super-resolution. In *Proceedings of the AAAI Conference on Artificial Intelligence*, volume 35, pages 1975–1983, 2021. [3](#)
- [30] Xin Li, Simeng Sun, Zhizheng Zhang, and Zhibo Chen. Multi-scale grouped dense network for vvc intra coding. In *Proceedings of the IEEE/CVF Conference on Computer Vision and Pattern Recognition Workshops*, pages 158–159, 2020. [1](#)
- [31] Xin Li, Zhizheng Zhang, Guoqiang Wei, Cuiling Lan, Wenjun Zeng, Xin Jin, and Zhibo Chen. Confounder identification-free causal visual feature learning. *arXiv preprint arXiv:2111.13420*, 2021. [3](#)
- [32] Yanghao Li, Hanzi Mao, Ross Girshick, and Kaiming He. Exploring plain vision transformer backbones for object detection. *arXiv preprint arXiv:2203.16527*, 2022. [3](#)
- [33] Yu Li, Robby T Tan, Xiaojie Guo, Jiangbo Lu, and Michael S Brown. Rain streak removal using layer priors. In *Proceedings of the IEEE conference on computer vision and pattern recognition*, pages 2736–2744, 2016. [7](#), [8](#), [16](#)
- [34] Jingyun Liang, Jiezhong Cao, Guolei Sun, Kai Zhang, Luc Van Gool, and Radu Timofte. Swinir: Image restoration using swin transformer. In *Proceedings of the IEEE/CVF International Conference on Computer Vision*, pages 1833–1844, 2021. [1](#), [3](#), [8](#), [15](#)
- [35] Jianzhao Liu, Jianxin Lin, Xin Li, Wei Zhou, Sen Liu, and Zhibo Chen. Lira: Lifelong image restoration from unknown blended distortions. In *European Conference on Computer Vision*, pages 616–632. Springer, 2020. [3](#)
- [36] Ze Liu, Yutong Lin, Yue Cao, Han Hu, Yixuan Wei, Zheng Zhang, Stephen Lin, and Baining Guo. Swin transformer: Hierarchical vision transformer using shifted windows. In *Proceedings of the IEEE/CVF International Conference on Computer Vision*, pages 10012–10022, 2021. [1](#), [3](#)
- [37] Andreas Lugmayr, Martin Danelljan, and Radu Timofte. Un-supervised learning for real-world super-resolution. In *2019 IEEE/CVF International Conference on Computer Vision Workshop (ICCVW)*, pages 3408–3416. IEEE, 2019. [2](#), [3](#)
- [38] Fangrui Lv, Jian Liang, Shuang Li, Bin Zang, Chi Harold Liu, Ziteng Wang, and Di Liu. Causality inspired representation learning for domain generalization. In *Proceedings of the IEEE/CVF Conference on Computer Vision and Pattern Recognition*, pages 8046–8056, 2022. [2](#), [3](#)
- [39] Divyat Mahajan, Shruti Tople, and Amit Sharma. Domain generalization using causal matching. In *International Conference on Machine Learning*, pages 7313–7324. PMLR, 2021. [2](#), [3](#)
- [40] David Martin, Charless Fowlkes, Doron Tal, and Jitendra Malik. A database of human segmented natural images and its application to evaluating segmentation algorithms and measuring ecological statistics. In *Proceedings Eighth IEEE International Conference on Computer Vision. ICCV 2001*, volume 2, pages 416–423. IEEE, 2001. [5](#), [6](#), [7](#)
- [41] Yusuke Matsui, Kota Ito, Yuji Aramaki, Azuma Fujimoto, Toru Ogawa, Toshihiko Yamasaki, and Kiyoharu Aizawa. Sketch-based manga retrieval using manga109 dataset. *Multimedia Tools and Applications*, 76(20):21811–21838, 2017. [5](#), [6](#), [7](#)
- [42] Sreyas Mohan, Zahra Kadkhodaie, Eero P Simoncelli, and Carlos Fernandez-Granda. Robust and interpretable blind image denoising via bias-free convolutional neural networks. *arXiv preprint arXiv:1906.05478*, 2019. [1](#), [3](#)
- [43] Seungjun Nah, Sanghyun Son, Jaerin Lee, and Kyoung Mu Lee. Clean images are hard to blur: Exploiting the ill-posed inverse task for dynamic scene deblurring. In *International Conference on Learning Representations*, 2021. [1](#), [3](#)
- [44] Alex Nichol, Joshua Achiam, and John Schulman. On first-order meta-learning algorithms. *arXiv preprint arXiv:1803.02999*, 2018. [5](#), [14](#), [15](#)
- [45] Seobin Park, Jinsu Yoo, Donghyeon Cho, Jiwon Kim, and Tae Hyun Kim. Fast adaptation to super-resolution networks via meta-learning. In *European Conference on Computer Vision*, pages 754–769. Springer, 2020. [1](#)
- [46] Judea Pearl. Causal inference in statistics: An overview. *Statistics surveys*, 3:96–146, 2009. [1](#), [2](#), [3](#), [13](#)
- [47] Tobias Plotz and Stefan Roth. Benchmarking denoising algorithms with real photographs. In *Proceedings of the IEEE conference on computer vision and pattern recognition*, pages 1586–1595, 2017. [7](#), [8](#), [16](#), [18](#)
- [48] Jae Woong Soh, Sunwoo Cho, and Nam Ik Cho. Meta-transfer learning for zero-shot super-resolution. In *Proceedings of the IEEE/CVF Conference on Computer Vision and Pattern Recognition*, pages 3516–3525, 2020. [1](#)
- [49] Robin Strudel, Ricardo Garcia, Ivan Laptev, and Cordelia Schmid. Segmenter: Transformer for semantic segmentation. In *Proceedings of the IEEE/CVF International Conference on Computer Vision*, pages 7262–7272, 2021. [3](#)
- [50] Wei Sun, Dong Gong, Qinfeng Shi, Anton van den Hengel, and Yanning Zhang. Learning to zoom-in via learning to zoom-out: Real-world super-resolution by generating and adapting degradation. *IEEE Transactions on Image Processing*, 30:2947–2962, 2021. [2](#), [3](#)

- [51] Radu Timofte, Eirikur Agustsson, Luc Van Gool, Ming-Hsuan Yang, and Lei Zhang. Ntire 2017 challenge on single image super-resolution: Methods and results. In *Proceedings of the IEEE conference on computer vision and pattern recognition workshops*, pages 114–125, 2017. 2, 8, 15, 16
- [52] Phong Tran, Anh Tuan Tran, Quynh Phung, and Minh Hoai. Explore image deblurring via encoded blur kernel space. In *Proceedings of the IEEE/CVF Conference on Computer Vision and Pattern Recognition*, pages 11956–11965, 2021. 3
- [53] Zhengzhong Tu, Hossein Talebi, Han Zhang, Feng Yang, Peyman Milanfar, Alan Bovik, and Yinxiao Li. Maxim: Multi-axis mlp for image processing. In *Proceedings of the IEEE/CVF Conference on Computer Vision and Pattern Recognition*, pages 5769–5780, 2022. 1, 3
- [54] Hua Wang, Dewei Su, Chuangchuang Liu, Longcun Jin, Xianfang Sun, and Xinyi Peng. Deformable non-local network for video super-resolution. *IEEE Access*, 7:177734–177744, 2019. 5
- [55] Menglu Wang, Xueyang Fu, Zepi Sun, and Zheng-Jun Zha. Jpeg artifacts removal via compression quality ranker-guided networks. In *Proceedings of the Twenty-Ninth International Conference on International Joint Conferences on Artificial Intelligence*, pages 566–572, 2021. 1
- [56] Tan Wang, Jianqiang Huang, Hanwang Zhang, and Qianru Sun. Visual commonsense representation learning via causal inference. In *Proceedings of the IEEE/CVF Conference on Computer Vision and Pattern Recognition Workshops*, pages 378–379, 2020. 2, 3
- [57] Xintao Wang, Liangbin Xie, Chao Dong, and Ying Shan. Real-esrgan: Training real-world blind super-resolution with pure synthetic data. In *Proceedings of the IEEE/CVF International Conference on Computer Vision*, pages 1905–1914, 2021. 2, 5, 7, 8, 16
- [58] Xintao Wang, Ke Yu, Shixiang Wu, Jinjin Gu, Yihao Liu, Chao Dong, Yu Qiao, and Chen Change Loy. Esrgan: Enhanced super-resolution generative adversarial networks. In *Proceedings of the European conference on computer vision (ECCV) workshops*, pages 0–0, 2018. 1, 5, 8
- [59] Pengxu Wei, Hannan Lu, Radu Timofte, Liang Lin, Wangmeng Zuo, Zhihong Pan, Baopu Li, Teng Xi, Yanwen Fan, Gang Zhang, et al. Aim 2020 challenge on real image super-resolution: Methods and results. In *Computer Vision—ECCV 2020 Workshops: Glasgow, UK, August 23–28, 2020, Proceedings, Part III 16*, pages 392–422. Springer, 2020. 1
- [60] Pengxu Wei, Hannan Lu, Radu Timofte, Liang Lin, Wangmeng Zuo, Zhihong Pan, Baopu Li, Teng Xi, Yanwen Fan, Gang Zhang, et al. Aim 2020 challenge on real image super-resolution: Methods and results. In *European Conference on Computer Vision*, pages 392–422. Springer, 2020. 3
- [61] Pengxu Wei, Ziwei Xie, Hannan Lu, Zongyuan Zhan, Qixiang Ye, Wangmeng Zuo, and Liang Lin. Component divide-and-conquer for real-world image super-resolution. In *European Conference on Computer Vision*, pages 101–117. Springer, 2020. 7, 8, 16
- [62] Yunxuan Wei, Shuhang Gu, Yawei Li, Radu Timofte, Longcun Jin, and Hengjie Song. Unsupervised real-world image super resolution via domain-distance aware training. In *Proceedings of the IEEE/CVF Conference on Computer Vision and Pattern Recognition*, pages 13385–13394, 2021. 2, 3
- [63] Ren Yang, Radu Timofte, Xin Li, Qi Zhang, Lin Zhang, Fanglong Liu, Dongliang He, He Zheng, Weihang Yuan, Pavel Ostyakov, et al. Aim 2022 challenge on super-resolution of compressed image and video: Dataset, methods and results. *arXiv preprint arXiv:2208.11184*, 2022. 3
- [64] Wenhan Yang, Robby T Tan, Jiashi Feng, Jiaying Liu, Zongming Guo, and Shuicheng Yan. Deep joint rain detection and removal from a single image. In *Proceedings of the IEEE conference on computer vision and pattern recognition*, pages 1357–1366, 2017. 7, 8, 16
- [65] Xu Yang, Hanwang Zhang, Guojun Qi, and Jianfei Cai. Causal attention for vision-language tasks. In *Proceedings of the IEEE/CVF Conference on Computer Vision and Pattern Recognition*, pages 9847–9857, 2021. 2, 3
- [66] Ke Yu, Chao Dong, Liang Lin, and Chen Change Loy. Crafting a toolchain for image restoration by deep reinforcement learning. In *Proceedings of the IEEE conference on computer vision and pattern recognition*, pages 2443–2452, 2018. 16
- [67] Zhongqi Yue, Qianru Sun, Xian-Sheng Hua, and Hanwang Zhang. Transporting causal mechanisms for unsupervised domain adaptation. In *Proceedings of the IEEE/CVF International Conference on Computer Vision*, pages 8599–8608, 2021. 2, 3
- [68] Zhongqi Yue, Hanwang Zhang, Qianru Sun, and Xian-Sheng Hua. Interventional few-shot learning. *Advances in neural information processing systems*, 33:2734–2746, 2020. 2, 3
- [69] Syed Waqas Zamir, Aditya Arora, Salman Khan, Munawar Hayat, Fahad Shahbaz Khan, and Ming-Hsuan Yang. Restormer: Efficient transformer for high-resolution image restoration. In *Proceedings of the IEEE/CVF Conference on Computer Vision and Pattern Recognition*, pages 5728–5739, 2022. 3
- [70] Syed Waqas Zamir, Aditya Arora, Salman Khan, Munawar Hayat, Fahad Shahbaz Khan, Ming-Hsuan Yang, and Ling Shao. Multi-stage progressive image restoration. In *Proceedings of the IEEE/CVF conference on computer vision and pattern recognition*, pages 14821–14831, 2021. 15, 16
- [71] Roman Zeyde, Michael Elad, and Matan Protter. On single image scale-up using sparse-representations. In *International conference on curves and surfaces*, pages 711–730. Springer, 2010. 6
- [72] He Zhang and Vishal M Patel. Density-aware single image de-raining using a multi-stream dense network. In *Proceedings of the IEEE conference on computer vision and pattern recognition*, pages 695–704, 2018. 8, 16
- [73] He Zhang, Vishwanath Sindagi, and Vishal M Patel. Image de-raining using a conditional generative adversarial network. *IEEE transactions on circuits and systems for video technology*, 30(11):3943–3956, 2019. 7, 8, 16
- [74] Kai Zhang, Jingyun Liang, Luc Van Gool, and Radu Timofte. Designing a practical degradation model for deep blind image super-resolution. In *Proceedings of the IEEE/CVF International Conference on Computer Vision*, pages 4791–4800, 2021. 2, 7, 8

- [75] Lei Zhang, Xiaolin Wu, Antoni Buades, and Xin Li. Color demosaicking by local directional interpolation and nonlocal adaptive thresholding. *Journal of Electronic imaging*, 20(2):023016, 2011. [5](#), [6](#)
- [76] Yi Zhang, Dasong Li, Ka Lung Law, Xiaogang Wang, Hongwei Qin, and Hongsheng Li. Idr: Self-supervised image denoising via iterative data refinement. In *Proceedings of the IEEE/CVF Conference on Computer Vision and Pattern Recognition*, pages 2098–2107, 2022. [3](#)
- [77] Yulun Zhang, Kunpeng Li, Kai Li, Lichen Wang, Bineng Zhong, and Yun Fu. Image super-resolution using very deep residual channel attention networks. In *Proceedings of the European conference on computer vision (ECCV)*, pages 286–301, 2018. [3](#)
- [78] Yulun Zhang, Yapeng Tian, Yu Kong, Bineng Zhong, and Yun Fu. Residual dense network for image restoration. *IEEE Transactions on Pattern Analysis and Machine Intelligence*, 43(7):2480–2495, 2020. [1](#), [3](#)

Appendix

Section 7 provides the systematic introduction for the related notations of the back-door criterion in causal learning. Section 8 explains the counterfactual distortion augmentation from the causality perspective.

Section 9 theoretically derives the parallel sampling in Eq. 5 of our paper.

Section 10 clarifies the implementations of four variants of our DIL, which can help the readers to reproduce our methods more easily.

Section 11 describes the more detailed experimental settings and the construction of distortion/confounder set D in different image restoration tasks.

Section 12 visualizes more subjective comparisons on different image restoration tasks.

7. The Back-door Criterion in Causality.

In this section, we clarify the related notations and derivations for the back-door criterion in causality.

Structure causal Model. As described in [18, 46], we can describe the causal relationship between different vectors with a directed Structural causal Model (SCM) like Fig. 7. A directed arrow $X \rightarrow Y$ represent X is the cause of the Y . The difference between correlation and causation is as follows: 1) In causation, given $X \rightarrow Y$, changing the X will cause the effect on Y . But changing Y does not have an effect on X since Y is not the cause of X . 2) In correlation, we can compute the correlation between X and Y with conditional probability $P(Y|X)$ and $P(X|Y)$ no matter whether there is causation between X and Y . In general, model training in deep learning is a process to fit the correlation between inputs and their labels instead of the causation.

Confounder. The confounder is defined based on the SCM, which represents the variables (e.g., C in Fig. 7) that are the common cause between two other variables (e.g., X and Y in Fig. 7). The fork connection $X \leftarrow C \rightarrow Y$ causes the spurious correlation for X and Y , which has a confounding effect on the estimation of the causal relationship between X and Y . In other words, the correlation between X and Y learned by the model also is implicitly conditioned on the confounder C .

do operation. A *do* operation means to cut off the connection from the $C \rightarrow X$, which is shown in Fig. 8. In this way, the correlation introduced from the path $X \leftarrow C \rightarrow Y$ is removed from *do* operation. Then the correlation learned by the model is only from the $X \rightarrow Y$, which are represented as $P(Y|do(X))$. And this causal correlation is independent of the confounder C and is what we expect the model to learn.

Back-door criterion. The back-door criterion is proposed in [18, 46], which aims to implement the *do* operation and eliminate the spurious correlation existed in $X \leftarrow C \rightarrow$

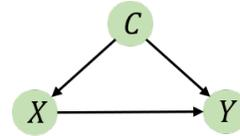


Figure 7. A structural causal model for back-door structure.

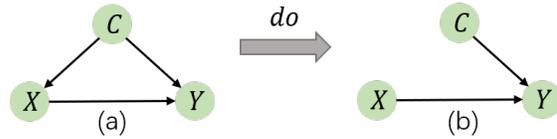


Figure 8. Back-door Criterion in Causality.

Y . It removes the confounding effects of confounder C by computing the average causal effects between $X \rightarrow Y$ by traversing all values of C as:

$$P(Y|do(X)) = \sum_c P(Y|X, C = c)P(C = c) \quad (6)$$

Based on Eq. 6, we can achieve the *do* operation in Fig. 8 (b).

The back-door criterion in Image Restoration As shown in Fig. 2 in our paper, we model the image restoration process as a structural causal model, where $D = \{d_i | 1 \leq i \leq n\}$ are the confounders between the distorted images I_d and the expected reconstruction images I_o , which satisfies the back-door criterion. Therefore, we can derive the back-door criterion in image restoration as:

$$P(I_o|do(I_d)) = \sum_{i=1}^n P(I_o|I_d, D = d_i)P(D = d_i) \quad (7)$$

8. A proof for counterfactual distortion augmentation.

The counterfactuals aims to answer the question “if X been x , in the situation U , what $Y_{X=x}(U)$ would be?”. The three variables are in the same structural causal model (SCM), and X and U are the cause of Y . As described in [18, 46], the calculating of counterfactuals follows three steps: 1) Abduction: Use evidence e to determine the value of U . 2) Action: Remove the structural equations for the variables X to modify the model M (i.e., the SCM). Then, set the X as $X = x$ to obtain the modified M_x . 3) Prediction: Use the M_x and $U = u$ to compute the value of Y (i.e., the consequence of the counterfactual).

Considering the generation process of the distorted images $I_d = g(I_c, d)$, where I_c and d are the clean images and distortion type/degree, respectively. g is the degradation process. The generation process can be modeled as a

structural causal model $I_c \rightarrow I_d \leftarrow d$. To construct the datasets for the training of DIL, it is better to collect various distorted/clean image pairs with different distortions but the same content. However, in the real world, it is non-trivial to collect the datasets to satisfy this. Therefore, we can construct the ideal datasets by answering the counterfactual question “if D is d_i , what the I_d would be with I_c invariant?”. We call the construction counterfactual distortion augmentation.

Analogously, the computing of counterfactuals in distortion augmentation follows a three-step procedure. 1) Abduction: Use the distorted image I_d to determine the value of I_c , i.e., $P(I_c|I_d)$. 2) Action: Modify the degradation model, g , so that D is adjusted to the counterfactual value d_i , that might rarely existed in real-world (e.g., the synthesised distortions). 3) Prediction: Compute the consequence I_{d_i} of the counterfactual based on estimated I_c and modified degradation model g_{d_i} .

It is fortunate that there are amounts of high-quality images captured by professional devices, that are only degraded by some extremely mild distortions. We can regard these images as clean images I_c . Therefore, the first step in counterfactuals is unnecessary and can be ignored. We can implement the counterfactual distortion augmentation by adding different synthetic distortion types or degrees to the same image contents I_c .

9. The derivation of the parallel sampling.

In this section, we will give the derivation of our parallel sampling in Eq. 5 of our paper. From Eq. 3 and Eq. 4 in our paper as:

$$\theta^* = \arg \min_{\theta} \mathbb{E}_{(I_d, I_c) \sim \mathcal{D}} \left[\frac{1}{n} \sum_{d_i \in D} \mathcal{L}(f_{\phi_{d_i}}(I_d), I_c) \right], \quad (8)$$

where $\phi_{d_i} = \theta - \alpha \nabla_{\theta} \mathcal{L}(f_{\theta}(I_{d_i}), I_c)$

we can conduct the Taylor expansion for the above equation at position θ as:

$$\begin{aligned} \theta^* &= \arg \min_{\theta} \mathbb{E}_{(I_d, I_c) \sim \mathcal{D}} \left\{ \frac{1}{n} \sum_{d_i \in D} [\mathcal{L}(f_{\theta}(I_d), I_c) \right. \\ &\quad \left. - \alpha \nabla_{\theta} \mathcal{L}(f_{\theta}(I_{d_i}), I_c) \nabla_{\theta} \mathcal{L}(f_{\theta}(I_d), I_c) \right. \\ &\quad \left. + o(\nabla_{\theta} \mathcal{L}(f_{\theta}(I_d), I_c))] \right\} \\ &= \arg \min_{\theta} \mathbb{E}_{(I_d, I_c) \sim \mathcal{D}} \{ \mathcal{L}(f_{\theta}(I_d), I_c) \\ &\quad - \frac{1}{n} \sum_{d_i \in D} \alpha [\nabla_{\theta} \mathcal{L}(f_{\theta}(I_{d_i}), I_c)] \nabla_{\theta} \mathcal{L}(f_{\theta}(I_d), I_c) \\ &\quad + o(\nabla_{\theta} \mathcal{L}(f_{\theta}(I_d), I_c))] \} \\ &= \arg \min_{\theta} \mathbb{E}_{(I_d, I_c) \sim \mathcal{D}} \{ \mathcal{L}(f_{\theta}(I_d), I_c) \\ &\quad - \alpha \nabla_{\theta} [\sum_{d_i \in D} \frac{1}{n} \mathcal{L}(f_{\theta}(I_{d_i}), I_c)] \nabla_{\theta} \mathcal{L}(f_{\theta}(I_d), I_c) \\ &\quad + o(\nabla_{\theta} \mathcal{L}(f_{\theta}(I_d), I_c))] \} \end{aligned} \quad (9)$$

Then we conduct the Taylor inverse expansion for the Eq. 9. The Eq. 9 can be derived as:

$$\theta^* = \arg \min_{\theta} \mathbb{E}_{(I_d, I_c) \sim \mathcal{D}} \left[\mathcal{L}(f_{\theta - \alpha \nabla_{\theta} \sum_{d_i \in D} \frac{1}{n} \mathcal{L}(f_{\theta}(I_{d_i}), I_c)}(I_d), I_c) \right] \quad (10)$$

Let $\phi_{\bar{d}} = \theta - \alpha \nabla_{\theta} \sum_{d_i \in D} \frac{1}{n} \mathcal{L}(f_{\theta}(I_{d_i}), I_c)$, we can obtain the final equation as Eq. 5 of our paper as:

$$\theta^* = \arg \min_{\theta} \mathbb{E}_{(I_d, I_c) \sim \mathcal{D}} [\mathcal{L}(f_{\phi_{\bar{d}}}(I_d), I_c)],$$

where $\phi_{\bar{d}} = \theta - \alpha \nabla_{\theta} \sum_{d_i \in D} \frac{1}{n} \mathcal{L}(f_{\theta}(I_{d_i}), I_c)$, (11)

10. The detailed algorithms on four variants of DIL.

We further demonstrate the algorithm details of four variants of our proposed DIL in the Alg. 1 (DIL_{ps}), Alg. 2 (DIL_{ss}), Alg. 3 (DIL_{pf}), and Alg. 4 (DIL_{sf}). As derived in Eq. 11, we can utilize the parallel data sampling for all distortions D to substitute the serial sampling based optimization. The implementation differences between the two sampling strategies can be observed by comparing the Line 5 – 6 in the Alg. 1 and Line 5 – 9 in the Alg. 2. We can find that parallel sampling can reduce the number of parameter updating by $1/n$. By comparing the Alg. 1 and Alg. 3, we can find that only first-order gradient existed in the DIL_{pf}, which is an approximation of the second-order optimization in Alg. 1. The related proof can be found in the [44].

11. Implementation Details.

11.1. Overall Settings.

For all image restoration tasks (except for the image deraining task) in this paper, we use 800 images from

Algorithm 1 DIL_{ps} (The variant of DIL with parallel sampling and second-order optimization)

- 1: **Input:** Training dataset $\mathcal{D} = \{I_{d_i}, I_c | 1 \leq i \leq n\}$, where n is number of distortion types and degrees (*i.e.*, confounders), and $D = \{d_i | 1 \leq i \leq n\}$ is the confounder set.
 - 2: **Init:** Restoration network f with the parameters θ , learning rate α for virtually updating, β for the training.
 - 3: **while** not converge **do**
 - 4: Sample training pairs (I_d, I_c) from D .
 - 5: Sample training pairs $\{I_{d_i}, I_c\}_{i=1}^n$ from \mathcal{D} .
 - 6: Virtual updating for the parameters θ as :

$$\phi_{\bar{d}} \leftarrow \theta - \alpha \nabla_{\theta} \sum_{d_i \in D} \frac{1}{n} \mathcal{L}(f_{\theta}(I_{d_i}), I_c).$$
 - 7: Updating the parameters θ with second-order gradient: $\theta \leftarrow \theta - \beta \mathcal{L}(f_{\phi_{\bar{d}}}(I_d), I_c)$
 - 8: **end while**
-

Algorithm 2 DIL_{ss} (The variant of DIL with serial sampling and second-order optimization)

- 1: **Input:** Training dataset $\mathcal{D} = \{I_{d_i}, I_c | 1 \leq i \leq n\}$, where n is number of distortion types and degrees (*i.e.*, confounders), and $D = \{d_i | 1 \leq i \leq n\}$ is the confounder set.
 - 2: **Init:** Restoration network f with the parameters θ , learning rate α for virtually updating, β for the training.
 - 3: **while** not converge **do**
 - 4: Sample training pairs (I_d, I_c) from D .
 - 5: **for** $1 \leq i \leq n$ **do**
 - 6: Sample training pairs (I_{d_i}, I_c) from \mathcal{D} .
 - 7: Virtual updating for the parameters θ :

$$\phi_{d_i} \leftarrow \theta - \alpha \nabla_{\theta} \mathcal{L}(f_{\theta}(I_{d_i}), I_c)$$
 - 8: Compute the loss for the second-order gradient:

$$\mathcal{L}(f_{\phi_{d_i}}(I_d), I_c)$$
 - 9: **end for**
 - 10: Updating the parameters θ with second-order gradient: $\theta \leftarrow \theta - \beta \frac{1}{n} \sum_{d_i \in D} \nabla_{\theta} \mathcal{L}(f_{\phi_{d_i}}(I_d), I_c)$
 - 11: **end while**
-

DIV2K [2] and 2650 images from Flickr2K [51] as the clean images to construct the datasets for training. Following the common setting [34, 70], In the training process, we randomly crop the distorted/clean image pairs with the size of 64×64 from the training images, and feed them to the restoration network to optimize the parameters. In the process of the counterfactual distortion augmentation, the distorted patches I_d are generated online according to distortion set D of different image restoration tasks. For ERM, we use Adam optimizer with $\beta_1 = 0.9$ and $\beta_2 = 0.999$. For DIL_{sf} and DIL_{pf} training paradigms, the same Adam op-

Algorithm 3 DIL_{pf} (The variant of DIL with parallel sampling and first-order optimization)

- 1: **Input:** Training dataset $\mathcal{D} = \{I_{d_i}, I_c | 1 \leq i \leq n\}$, where n is number of distortion types and degrees (*i.e.*, confounders), and $D = \{d_i | 1 \leq i \leq n\}$ is the confounder set.
 - 2: **Init:** Restoration network f with the parameters θ , learning rate α for virtually updating, β for the training.
 - 3: **while** not converge **do**
 - 4: $\tilde{\theta} \leftarrow \theta$
 - 5: **for** step=1 to 2 **do**
 - 6: Sample training pairs $\{I_{d_i}, I_c\}_{i=1}^n$ from \mathcal{D} .
 - 7: Virtual updating:

$$\tilde{\theta} \leftarrow \tilde{\theta} - \alpha \nabla_{\tilde{\theta}} \sum_{d_i \in D} \frac{1}{n} \mathcal{L}(f_{\tilde{\theta}}(I_{d_i}), I_c).$$
 - 8: **end for**
 - 9: Updating the parameters θ : $\theta \leftarrow \theta - \beta(\tilde{\theta} - \theta)$
 - 10: **end while**
-

Algorithm 4 DIL_{sf} (The variant of DIL with serial sampling and first-order optimization)

- 1: **Input:** Training dataset $\mathcal{D} = \{I_{d_i}, I_c | 1 \leq i \leq n\}$, where n is number of distortion types and degrees (*i.e.*, confounders), and $D = \{d_i | 1 \leq i \leq n\}$ is the confounder set.
 - 2: **Init:** Restoration network f with the parameters θ , learning rate α for virtually updating, β for the training.
 - 3: **while** not converge **do**
 - 4: $\tilde{\theta} \leftarrow \theta$
 - 5: **for** $1 \leq i \leq n$ **do**
 - 6: Sample training pairs (I_{d_i}, I_c) from \mathcal{D} .
 - 7: Virtual Updating: $\tilde{\theta} \leftarrow \tilde{\theta} - \alpha \nabla_{\tilde{\theta}} \mathcal{L}(f_{\tilde{\theta}}(I_{d_i}), I_c)$
 - 8: **end for**
 - 9: Updating the parameters θ : $\theta \leftarrow \theta - \beta(\tilde{\theta} - \theta)$
 - 10: **end while**
-

timizer with ERM is used for the training optimization for the above two variants. For the virtual updating process, we adopt the Adam optimizer with $\beta_1 = 0$ and $\beta_2 = 0.999$ following [44]. For DIL_{ss} and DIL_{ps}, we utilize the same two Adam optimizers as that used in ERM for the virtual updating step and training optimization step. We set the batch size to 8 on each GPU. The total training iterations and initial learning rate are set to 400K and 1e-4, respectively. The learning rate will reduce by half at [200K, 300K]. All the tasks are optimized with the L1 loss if not mentioned. In the image deraining task, we utilize Charbonnier [7] Loss as:

$$\mathcal{L}_{char} = \sqrt{\|I_o - I_c\|^2 + \epsilon^2} \quad (12)$$

where I_o and I_c denotes the reconstructed images and clean images, respectively. Following previous works [23, 70], we set ϵ to $1e-3$.

11.2. The distortion/confounders set D for different tasks.

In this section, we describe the specific construction of the distortion/confounder set D in the counterfactual distortion augmentation strategy.

11.2.1 Cross distortion degrees

Image Denoising. For image denoising, the distortion/confounder set is composed of Additive White Gaussian Noise (AWGN) with the noise intensity of [5, 10, 15, 20], which is added to the clean images from DF2K [2, 51] to construct the training data. For testing, we utilize several unseen noise intensities, including [30, 40, 50] to estimate the generalization capability of different schemes.

Image Deblurring. For image deblurring, we obtain I_d by applying the distortion/confounding set D to I_c , which contains the 2D gaussian filter with different blurring sigma of [1.0, 2.0, 3.0, 4.0]. For testing, we validate the generalization capability of different schemes on the sigma [4.2, 4.4, 4.6, 4.8, 5.0].

Hybrid distortion restoration. Following the [28, 66], the hybrid distortions are degraded with the superposition of blur, noise, and Jpeg compression artifacts in a sequence manner. The distortion/confounder set D for training is composed of multiple levels of severe hybrid distortions. The test datasets are composed of unseen distortion levels, including mild and moderate hybrid distortions.

11.2.2 Cross distortion types

Real Image Super-resolution. For real image super-resolution, we utilize the degradation model introduced by [57] for training. To simplify the training process, we adopt the one-order distortion synthesis mode in [57] to construct the distortion/confounder set D , where different $d_i \in D$ are divided with different noise types and blur types in the degradation model of [57]. To validate the generalization capability of different schemes for the “cross distortion types”, we exploit the RealSR [5] and DRealSR [61] for the real image super-resolution as our test data.

Real Image Denoising. For real image denoising, we obtain I_d based on the ISP process introduced by [19]. We divide this degradation model into four different distortion types based on the different color filter arrays (CFA) to construct D . We follow previous works [1, 47] and utilize real denoising datasets DND [47] and SIDD [1] as the benchmarks to validate the generalization capability of different schemes.

Image Deraining. For image deraining, we utilize three datasets with three different raining types, including Rain14000 [17], DID-MDN [72], and Heavy Rain Dataset [27], to construct the training data \mathcal{D} , and test the generalization capability of the restoration network on other three unseen raining types, including 100 rainy images from Rain100L [64], 100 rainy images from Rain800 [73], and 12 rainy images from Rain12 [33]. It is noteworthy that the synthesis strategies of the above raining types are rarely released. Therefore, in this task, we relax the content consistency between different raining types for training. And our DIL is still effective for improving the generalization capability of the restoration network.

12. More Subjective Visualization

We provide more visual comparisons for different image restoration tasks in this section. As shown in Fig. 9, the commonly-use ERM and our proposed DIL all achieve similar reconstructed results on the seen noise level ($\sigma = 15$). But ERM fails to restore high-quality images on unseen noise levels well, (e.g., $\sigma = 40$ and $\sigma = 50$), which indicates that ERM lacks of enough generalization ability for the unseen distortion degrees. In contrast, our DIL_{sf} can recover noise-free and structure-preserved images despite the distortion degrees do not exist in the training data. This further proves the correctness and effectiveness of our proposed DIL.

We show more visual comparisons of image deblurring in Fig. 10. When dealing with unseen blur degrees, our proposed DIL can restore the clear structures, while ERM produces overshooting artifacts on the edges. More visualizations for real image denoising can be found in Fig. 11. And more visualizations for image deraining can be found in Fig. 12. We also visualize the subjective comparisons on hybrid-distorted image restoration in Fig. 13.

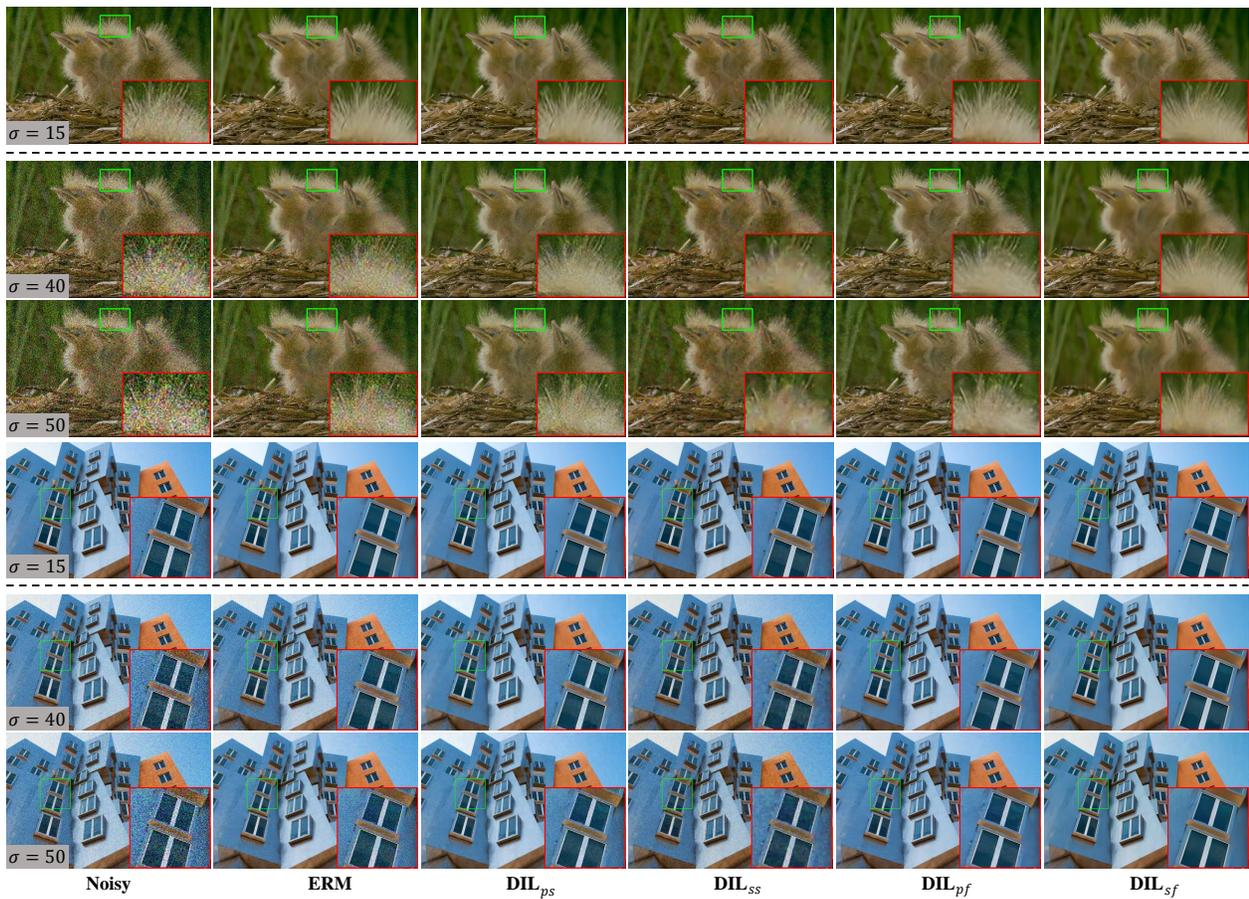


Figure 9. Visual comparison of the commonly-used ERM and our proposed four variants of DIL on image denoising task. The noise level above the dash line is seen, while noise levels below are unseen.

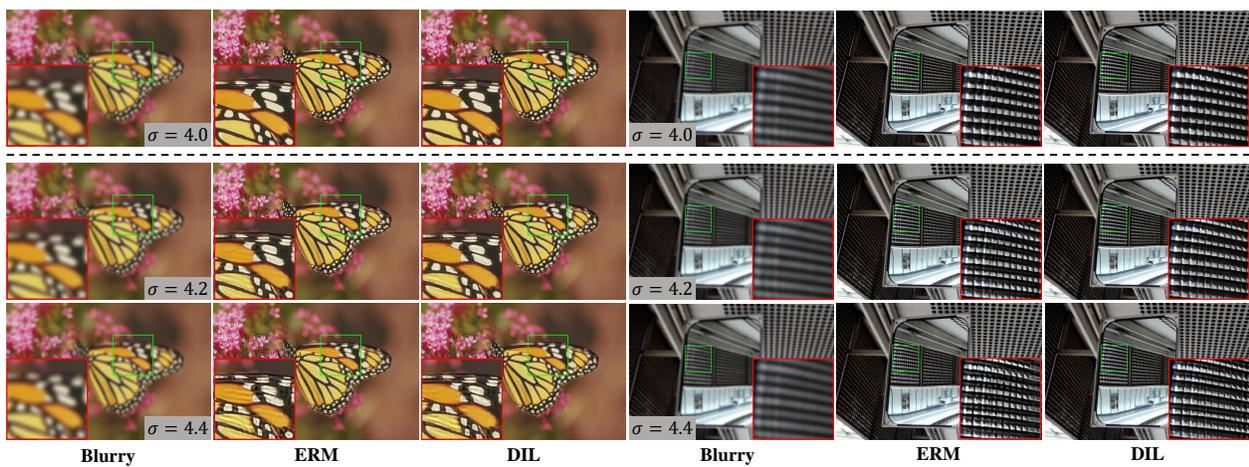


Figure 10. Visual comparison of the commonly-used ERM and DIL on image deblurring task. The blur level above the dash line is seen, while blur levels below are unseen.

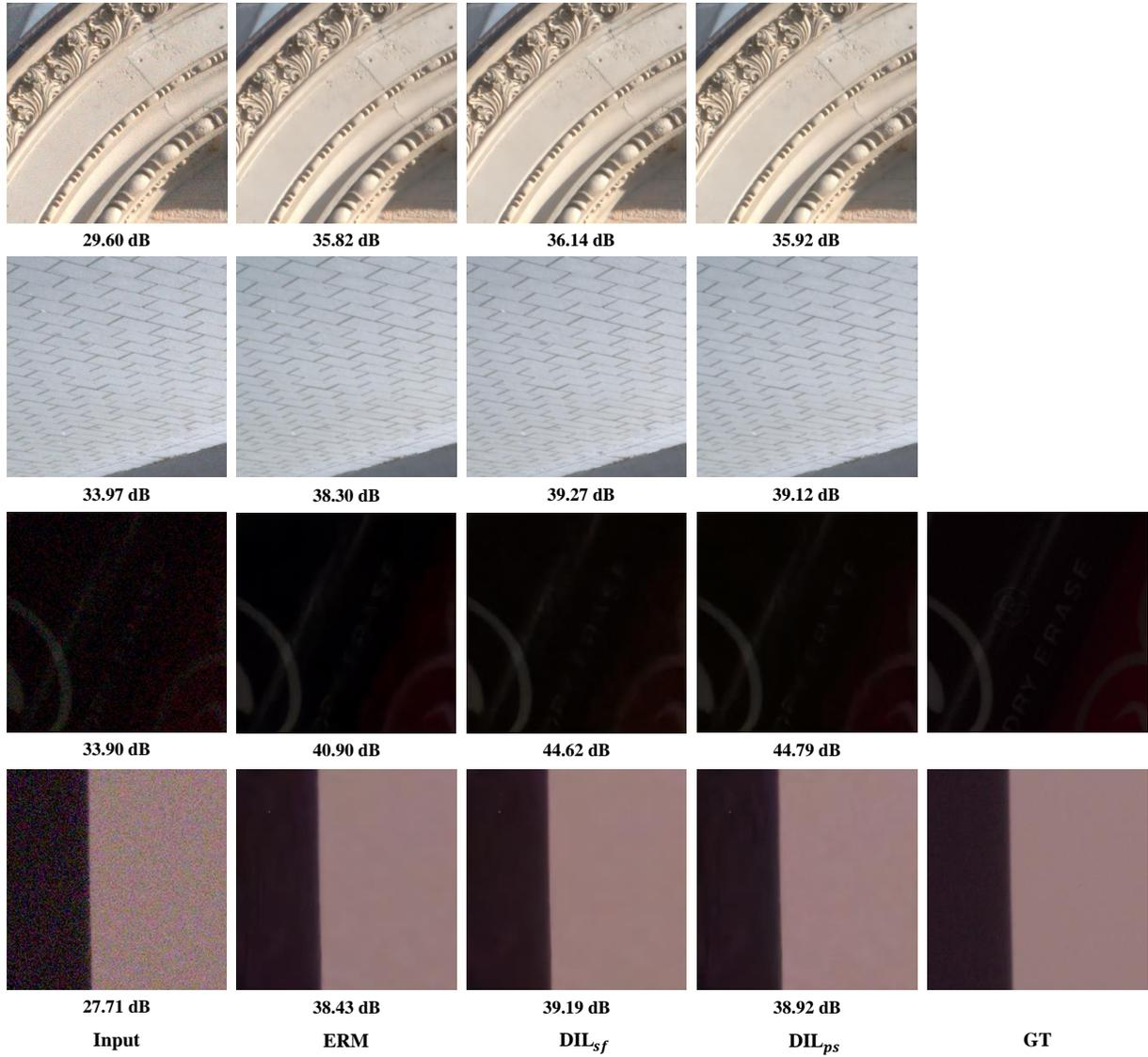


Figure 11. Visual comparison of the commonly-used ERM and DIL on real image denoising task. The top samples are from DND [47] while the bottom samples are from SIDD [1]. Brightening the third line for a better view.

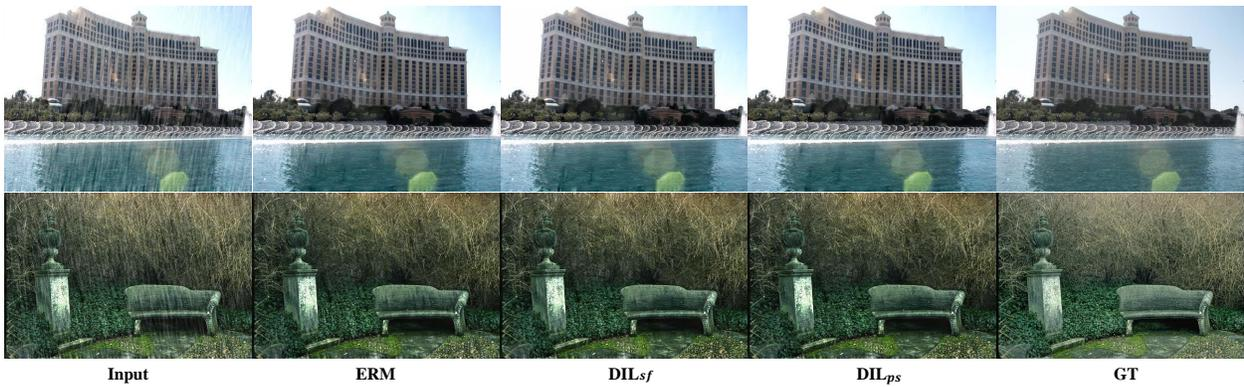


Figure 12. Visual comparison of the commonly-used ERM, our DIL_{sf} and DIL_{ps} on image deraining task.



Figure 13. Visual comparison of the commonly-used ERM and DIL on hybrid distortion removal task. Here, we show restoration results on the mild distortion level, which is the unseen distortion level for the restoration network.